



Article

Influence of Fin Length on Magneto-Combined Convection Heat Transfer Performance in a Lid-Driven Wavy Cavity

Md. Fayz-Al-Asad ¹, Mehmet Yavuz ^{2,3,*}, Md. Nur Alam ⁴, Md. Manirul Alam Sarker ¹ and Omar Bazighifan ^{5,6}

¹ Department of Mathematics, Bangladesh University of Engineering and Technology (BUET), Dhaka 1000, Bangladesh; mdfayzalasad@pg.math.buet.ac.bd (M.F.-A.-A.); masarker@math.buet.ac.bd (M.M.A.S.)

² Department of Mathematics and Computer Sciences, Faculty of Science, Necmettin Erbakan University, Konya 42090, Turkey

³ Department of Mathematics, College of Engineering, Mathematics and Physical Sciences, University of Exeter, Cornwall TR10 9FE, UK

⁴ Department of Mathematics, Pabna University of Science & Technology, Pabna 6600, Bangladesh; nuralam23@pust.ac.bd

⁵ Section of Mathematics, International Telematic University Uninettuno, Corso Vittorio Emanuele II, 39, 00186 Rome, Italy; o.bazighifan@gmail.com

⁶ Department of Mathematics, Faculty of Science, Hadhramout University, Hadhramout 50512, Yemen

* Correspondence: m.yavuz@exeter.ac.uk



Citation: Fayz-Al-Asad, M.; Yavuz, M.; Alam, M.N.; Sarker, M.M.A.; Bazighifan, O. Influence of Fin Length on Magneto-Combined Convection Heat Transfer Performance in a Lid-Driven Wavy Cavity. *Fractal Fract.* **2021**, *5*, 107. <https://doi.org/10.3390/fractfract5030107>

Academic Editors: Praveen Agarwal, Hari Mohan Srivastava, Taekyun Kim and Shaher Momani

Received: 17 August 2021

Accepted: 29 August 2021

Published: 31 August 2021

Abstract: In the existent study, combined magneto-convection heat exchange in a driven enclosure having vertical fin was analyzed numerically. The finite element system-based GWR procedure was utilized to determine the flow model's governing equations. A parametric inquiry was executed to review the influence of Richardson and Hartmann numbers on flow shape and heat removal features inside a frame. The problem's resulting numerical outcomes were demonstrated graphically in terms of isotherms, streamlines, velocity sketches, local Nusselt number, global Nusselt number, and global fluid temperature. It was found that the varying lengths of the fin surface have a substantial impact on flow building and heat line sketch. Further, it was also noticed that a relatively fin length is needed to increase the heat exchange rate on the right cool wall at a high Richardson number. The fin can significantly enhance heat removal performance rate from an enclosure to adjacent fluid.

Keywords: finite element method; magnetic field; mixed convection; wavy cavity and fin surface

MSC: 35E05; 35C08; 35Q51; 37L50; 37J25; 33F05

1. Introduction

In computational fluid dynamics mechanisms, laminar mixed convection heat transfers in a lid driven cavity has drawn interest by the researchers because of its wide scope of applications. Numerous researchers have paid attention to the lid driven square shape enclosure, both from theoretical and engineering viewpoints. Azizul et al. [1] explored the influence on mixed convection in a wavy frame filled with nanofluids via a heat line idea. The demographic results confirm that the Richardson number larger values and Reynolds number improve heat exchange rate. Das and Mahmud [2] have probed natural convection inside a wavy frame cavity. Their outcomes depicted that amplitude and undulation numbers of a wavy surface modify heat alteration components inside an enclosure. Misirlioglu et al. [3] scrutinized natural convection through an inclined wavy porous cavity. Amiri et al. [4] reported the influence on wavy base wall on mixed convection heat variation in a lid driven frame. They evaluated the impact of undulation number, Richardson number (Ri), and suitability of a wavy wall on flow formation and heat transfer features. Rostami [5] numerically simulated the natural convection inside vertical wavy



Copyright: © 2021 by the authors. Licensee MDPI, Basel, Switzerland. This article is an open access article distributed under the terms and conditions of the Creative Commons Attribution (CC BY) license (<https://creativecommons.org/licenses/by/4.0/>).

walls enclosure throw unsteady case. Mansour et al. [6] examined natural convection within the wavy shape porous enclosure into the impact of thermic radiation applying a heated non-equilibrium model. Mushate [7] analyzed CFD prognostic on natural convection by an undulating porous enclosure. The outcomes exposed that heat alteration rate gains as the Rayleigh number increases and reductions with a rise in amplitude. Nada and Chamkha [8] investigated mixed convection in a nanofluid flow within wavy shape enclosure. They noticed that the heat substitution rate rises with a volume fraction of nano-particles concerning base surface geometry ratios and Richardson number. Sheremet and Pop [9] reviewed natural convection in a wavy surface porous enclosure with a sinusoidal condition on both level surface walls, including a nanofluid applying Buongiorno's mathematical representation. Sheremet et al. [10] studied free convective flow into a non-uniform heated undulating frame porous enclosure having a nanofluid flow supporting the influences of Brownian dispersion and thermophoresis. Cheong et al. [11] examined the natural convective in porous wavy structure, including sinusoidal heated and internal heat generation. Recently, Asad et al. [12,13] inquired heat transfer inquiry on convection for an in a triangular and wavy structure enclosure. Alsabery et al. [14] scrutinized a revolving solid cylinder's performance on entropy generation with heat transfer in a wavy shape framework porous cavity heated below.

The magnetic domain influence of an electrically transferring fluid on heat transfer and fluid movement is encountered in multiple engineering applications such as purification of molten metal's, cooling of nuclear reactors, MHD power generators, micro MHD pumps, liquid metal flow control, biological transportation, etc. Washing machines, blenders, vacuum cleaners, etc. have electric devices that work by magnetic principles. Rahman et al. [15] studied the conjugate impact of MHD and joule heating convection in a lid-driven square enclosure. They pointed that Hartmann number (Ha) Joule heating parameters have a notable influence on flow design and heat variation. Öztürk et al. [16] analyzed mixed convection in the presence of a field within a nanofluid-filled and non-uniform hot wavy wall lid-driven structure. They explained that the heat removal rate declined with a growing Hartmann number. Moreover, the heat substitution rate can increase or decrease by rises in the nanoparticles based on the Hartmann (Ha) and Richardson numbers. Ashorynejad and Shahriari [17] studied magneto-convection of a composite nanofluid inside an open wavy frame cavity. They obeyed that a Nusselt number diminishes with an augmentation of a Hartmann number, but it progresses by growing Rayleigh number and size of a nanoparticles. More recent inquiries related to wavy-, square-, and triangular-shaped enclosures within the influence of a magnetic field are available in [18–21].

Additionally, various engineering applications, including a fin such as a radiator in a car, heat transfer in power plants, computer CPU heat sinks, and heat transfer devices, were investigated by Gupta and Garu [22]. Moreover, the latest technology such as hydrogen fuel cells and fennec canines performing as fins discharges heat from the blood that passes through them. Nag et al. [23] examined natural convection with a non-uniform thermal cavity with a horizontal separation on the heated wall. Tasnim and Collins [24] scrutinized free convection heat transfer in a square enclosure joining a baffle on a heated wall. They noticed that the influence of the fin place on heat removal rate was heavily affected by fin length and Rayleigh number. Sun et al. [25] examined mixed convection in a lid-driven enclosure utilizing triangular conductive fins. They mentioned that a triangular fin is a suitable control parameter for flow construction and speed of heat transference. Xu et al. [26] explored the impact of fins and their height on natural convection inside the transition cavity. They decided that the stream near the finned surface transitions from steady to periodical unsteady flow at critical Ra sensitive to fin length. Elatar et al. [27] produced on laminar natural convection in a square frame, attaching a unique horizontal baffle in different locations and lengths attached to a heated surface. They reviewed the impact of fin locations and lengths of the frame on flow construction and heat removal components. Palaniappan et al. [28] scrutinized the impact of parallel insulated baffles

inside open enclosures. Siddiqui et al. [29] considered mixed convection in the sliding wall cavity within a micro-polar liquid. By exploring the literature records, it was noticed that more activities relevant to the instant study are found in [30–32]. Recently, Fin related papers for different shape of enclosure are studied by Asad et al. [33–35]. Also, numerous investigations have been conveyed about non-linear PDE equations, which can be viewed [36–38].

To the best of the researchers' knowledge, it confirms that no query has been reviewed on the wavy enclosure having vertical fin. The influence of fin length on mixed convection heat transfer in the presence of a magnetic field in a lid-driven wavy wall enclosure attaching vertical fin was numerically scrutinized in this surviving study.

2. Mathematical Formulation

A wavy shape enclosure was estimated for the existing study with a physical model with boundary conditions, as displayed in Figure 1. The thermo-physical attributes of fluid are supposed to be fixed, except for density modification in a buoyancy expression, which is handled according to Boussinesq approximation, while the impacts of radiation and viscous diffusion are ignored. In general, the enclosure liquid is conjectured to be the Newtonian, incompressible, steady, and laminar flow.

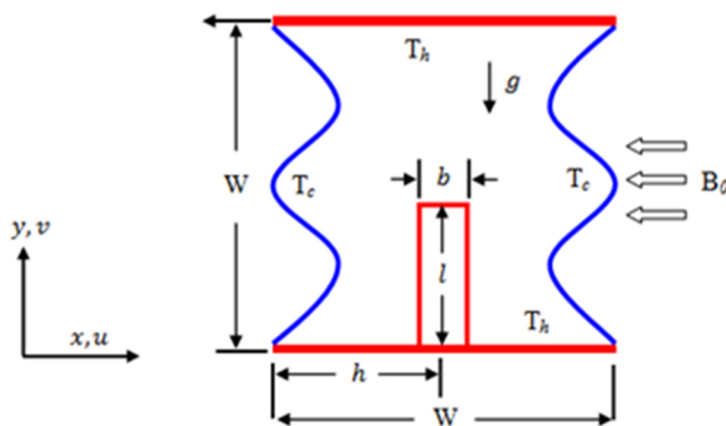


Figure 1. Schematic layout of wavy shape enclosure amidst boundary conditions.

Following the previous assumptions and the governing relevant equations by Öztop et al. [18], the dimensionless form is as follows:

$$\frac{\partial \psi}{\partial x} + \frac{\partial \varphi}{\partial y} = 0 \quad (1)$$

$$\rho \left(\psi \frac{\partial \psi}{\partial x} + \varphi \frac{\partial \psi}{\partial x} \right) = -\frac{\partial p}{\partial x} + \mu \nabla^2 \psi \quad (2)$$

$$\rho \left(\psi \frac{\partial \varphi}{\partial x} + \varphi \frac{\partial \varphi}{\partial x} \right) = -\frac{\partial p}{\partial y} + \mu \nabla^2 \varphi - \sigma \nu B_0^2 + \rho g \beta (T - T_c) \quad (3)$$

$$\left(\psi \frac{\partial T}{\partial x} + \varphi \frac{\partial T}{\partial x} \right) = \alpha \nabla^2 T \quad (4)$$

where ψ and φ are the velocity components along x and y directions, respectively, p is the pressure, ρ is the density, μ is the dynamic viscosity, β is the coefficient thermal expansion, σ is the electrical conductivity, B_0 is the magnetic field, T is the temperature, g is the gravitational force, $\mu = \rho v$ is the kinematic viscosity, and α is the thermal diffusivity.

2.1. Boundary Conditions

The boundary conditions for the present problem are specified as follows:

$$\text{On the top wall : } \psi = \psi_{lid}, \varphi = 0, T = T_h \quad (5)$$

$$\text{On the bottom wall : } \psi = \varphi = 0, T = T_h \quad (6)$$

$$\text{On the left surface : } \psi = \varphi = 0, T = T_c; A(1 - \cos(2\pi\lambda x)) \quad (7)$$

$$\text{On the right surface : } \psi = \varphi = 0, T = T_c; 1 - A(1 - \cos(2\pi\lambda x)) \quad (8)$$

$$\text{For fin surface : } 0 \leq y \leq l, \psi = \varphi = 0, T = T_h; x = h + \frac{b}{2} \text{ and } x = h - \frac{b}{2} \quad (9)$$

2.2. Dimensionless Analysis

Using the following dimensionless parameters, the governing equations can be converted to the dimensionless forms:

$$X = \frac{x}{W}; Y = \frac{y}{W}; \psi' = \frac{\psi_{lid} W}{\alpha}; \varphi' = \frac{\varphi W}{\alpha}; P = \frac{p W^2}{\rho \alpha^2}; H = \frac{h}{W}; L = \frac{l}{W} \text{ and } B = \frac{b}{W} \quad (10)$$

where X and Y are the coordinates varying along horizontal and vertical directions, ψ' and φ' are the velocity components in the X and Y directions, respectively, and P is the dimensionless pressure. After substitution of the dimensionless variables into Equations (1)–(4), we attained the following dimensionless equations:

$$\frac{\partial \psi'}{\partial X} + \frac{\partial \varphi'}{\partial Y} = 0 \quad (11)$$

$$\psi' \frac{\partial \psi'}{\partial X} + \varphi' \frac{\partial \psi'}{\partial Y} = - \frac{\partial P}{\partial X} + \frac{1}{Re} \nabla^2 \psi' \quad (12)$$

$$\psi' \frac{\partial \varphi'}{\partial X} + \varphi' \frac{\partial \varphi'}{\partial Y} = - \frac{\partial P}{\partial Y} + \frac{1}{Re} \nabla^2 \varphi' + Ri \theta - \frac{Ha^2 \varphi'}{Re} \quad (13)$$

$$\psi' \frac{\partial \theta}{\partial X} + \varphi' \frac{\partial \theta}{\partial Y} = \frac{1}{Pr Re} \nabla^2 \theta \quad (14)$$

The relevant parameters of the equations as mentioned above (1)–(4) are θ , Pr , Re , Gr , Ha , and Ri , which are individually represented as:

$$\theta = \frac{T_h - T_c}{\Delta T}, Pr = \frac{\nu}{\alpha}, Re = \frac{\psi_{lid} W}{\nu}, Gr = \frac{g \beta (T_h - T_c) W^3}{\nu^2}, Ha = B_0 W \sqrt{\frac{\sigma}{\mu}} \text{ and } Ri = \frac{Gr}{Re^2} \quad (15)$$

2.3. Dimensionless Boundary Conditions

$$\text{On the top wall : } \psi_{lid} = -1, \varphi' = 0, \theta = 1 \quad (16)$$

$$\text{On the bottom wall : } \psi' = \varphi' = 0, \theta = 1 \quad (17)$$

$$\text{On the left surface : } \psi' = \varphi' = 0, \theta = 0; A(1 - \cos(2\pi\lambda X)) \quad (18)$$

$$\text{On the right surface : } \psi' = \varphi' = 0, \theta = 0; 1 - A(1 - \cos(2\pi\lambda X)) \quad (19)$$

$$\text{For the fin surface : } 0 \leq Y \leq L, \psi' = \varphi' = 0; X = H + \frac{B}{2} \text{ and } X = H - \frac{B}{2} \quad (20)$$

2.4. Nusselt Number

Heat elimination via conduction was compared with heat elimination on the amount of convection as exhibited: $h * \Delta T = -k \frac{\partial T}{\partial n}$

By including the dimensionless parameters in Equation (15), we discovered the Nusselt number and global Nusselt number were established as:

$$Nu_L = - \frac{\partial \theta}{\partial N} \Big|_S \text{ and } Nu_{av} = \int_0^W \frac{\partial \theta}{\partial N} \Big|_S ds \quad (21)$$

3. Fin Effectiveness

Fin effectiveness is a variable that measures the heat conversion augmentation inside an enclosure where the fin is compared to a case without fin, defined by Elatar et al. [26] as follows:

$$\varepsilon_f = \frac{Q_{fin}}{Q_{without\ fin}} \quad (22)$$

4. Computational Outline

The relevant governing Equations (11)–(14) jointly amidst Equations (16)–(19) were prepared numerically employing a finite element operation with the Galerkin-weighted residual technique. Firstly, we used a penalty into finite element operation (FEO) by decreasing a pressure through penalty variable (γ), and incompressibility analyses are given of Equation (11) written as:

$$P = -\gamma \left(\frac{\partial \psi'}{\partial X} + \frac{\partial \varphi'}{\partial Y} \right) \quad (23)$$

Composing Equation (23), conservations of momentum Equations (12) and (13) were reduced to:

$$\psi' \frac{\partial \psi'}{\partial X} + \varphi' \frac{\partial \psi'}{\partial Y} = \gamma \left(\frac{\partial \psi'}{\partial X} + \frac{\partial \varphi'}{\partial Y} \right) + \frac{1}{Re} \nabla^2 \psi' \quad (24)$$

$$\psi' \frac{\partial \varphi'}{\partial X} + \varphi' \frac{\partial \varphi'}{\partial Y} = \gamma \left(\frac{\partial \psi'}{\partial X} + \frac{\partial \varphi'}{\partial Y} \right) + \frac{1}{Re} \nabla^2 \varphi' + Ri \theta - \frac{Ha^2 \varphi'}{Re} \quad (25)$$

Secondly, the evolution of momentum and energy Equations (24), (25), and (14) sequentially utilizing Equations (16)–(19) were arranged by choosing the Galerkin finite element scheme [39,40]. The engaging function approximating each stream pattern (ψ, φ) and heat features (θ) utilizing a primary set $\{\phi_i\}_{i=1}^k$ as:

$$\psi' \approx \sum_{i=1}^k \psi'_i \phi_i(X, Y); \quad \varphi' \approx \sum_{i=1}^k \varphi'_i \phi_i(X, Y) \quad \text{and} \quad \theta \approx \sum_{i=1}^k \theta_i \phi_i(X, Y) \quad (26)$$

The non-linear Equations (24), (25), and (14) were received via a Galerkin-weighted residual toward finite element tactics at the domain of inner nodes (Ω):

$$R_1^j \approx \sum_{i=1}^k \psi'_i \int_{\Omega} \left[\left(\sum_{i=1}^k \psi'_i \phi_i \right) \frac{\partial \phi_j}{\partial X} + \left(\sum_{i=1}^k \varphi'_i \phi_i \right) \frac{\partial \phi_j}{\partial Y} \right] \phi_j dX dY + \gamma \sum_{i=1}^k \psi'_i \int_{\Omega} \frac{\partial \phi_j}{\partial X} \frac{\partial \phi_i}{\partial X} dX dY \\ + \gamma \sum_{j=1}^k \varphi'_i \int_{\Omega} \frac{\partial \phi_j}{\partial X} \frac{\partial \phi_i}{\partial Y} dX dY + \frac{1}{Re} \sum_{i=1}^k \psi'_i \int_{\Omega} \left[\frac{\partial \phi_j}{\partial X} \frac{\partial \phi_i}{\partial X} + \frac{\partial \phi_j}{\partial Y} \frac{\partial \phi_i}{\partial Y} \right] dX dY \quad (27)$$

$$R_2^j \approx \sum_{i=1}^k \varphi'_i \int_{\Omega} \left[\left(\sum_{i=1}^k \psi'_i \phi_i \right) \frac{\partial \phi_j}{\partial X} + \left(\sum_{i=1}^k \varphi'_i \phi_i \right) \frac{\partial \phi_j}{\partial Y} \right] \phi_j dX dY + \gamma \sum_{i=1}^k \psi'_i \int_{\Omega} \frac{\partial \phi_j}{\partial Y} \frac{\partial \phi_i}{\partial X} dX dY \\ + \gamma \sum_{i=1}^k \varphi'_i \int_{\Omega} \frac{\partial \phi_j}{\partial Y} \frac{\partial \phi_i}{\partial Y} dX dY + \frac{1}{Re} \sum_{i=1}^k \psi'_i \int_{\Omega} \left[\frac{\partial \phi_j}{\partial X} \frac{\partial \phi_i}{\partial X} + \frac{\partial \phi_j}{\partial Y} \frac{\partial \phi_i}{\partial Y} \right] dX dY \\ + Ri \int_{\Omega} \left(\sum_{i=1}^k \theta_i \phi_i \right) \phi_j dX dY - \frac{Ha^2}{Re} \int_{\Omega} \left(\sum_{i=1}^k \varphi'_i \phi_i \right) \phi_j dX dY \quad (28)$$

$$R_3^j \approx \sum_{i=1}^k \theta_i \int_{\Omega} \left[\left(\sum_{i=1}^k \psi'_i \phi_i \right) \frac{\partial \phi_i}{\partial X} + \left(\sum_{i=1}^k \phi'_i \phi_i \right) \frac{\partial \phi_i}{\partial Y} \right] \phi_j dXdY + \frac{1}{PrRe} \sum_{i=1}^k \theta_i \int_{\Omega} \left[\frac{\partial \phi_j}{\partial X} \frac{\partial \phi_i}{\partial X} \right] dXdY \\ + \frac{1}{PrRe} \sum_{i=1}^k \theta_i \int_{\Omega} \left[\frac{\partial \phi_j}{\partial Y} \frac{\partial \phi_i}{\partial Y} \right] dXdY \quad (29)$$

where k , j , and i are the iteration, residual, nodes number, sequentially. The succeeding operations the beforehand Equations (27)–(29) were delivered through Gaussian quadrature system.

Lastly, Newton Raphson's iteration system was employed to discover residual equations iteratively. The detailed clarification may be located in earlier announced activities [12,28]. The convergence policies of the computational approach were performed once a subsequent convergence inquiry was provided as regards:

$$\left| \frac{\Pi^{n+1} - \Pi^n}{\Pi^{n+1}} \right| \leq 10^{-5} \quad (30)$$

5. Grid Refinement Test

To determine a proper grid size for the instant inquiry at $Ri = 1$, $Pr = 0.71$, $\lambda = 2$, $L = 0.45$, and $H = 0.50$, a grid refinement test was scrutinized with several mesh types. The average Nusselt number of fin surfaces is obtained in Table 1 and captured in Figure 2, exposing insignificant changes in the grid size: 6844 number of nodes and 13,273 sizes afforded an adequate solution for the present examination.

Table 1. Inquiry of grid refinement at $Ri = 1$, $\lambda = 2$, $Pr = 0.71$, $H = 0.50$, and $L = 0.45$.

Nodes (Elements)	931 (1700)	1213 (2245)	1823 (3421)	6844 (13,273)	25,133 (49,464)
Nu_{av}	5.1290	5.2303	5.3952	5.6491	5.6617
Time (s)	7	10	13	21	38

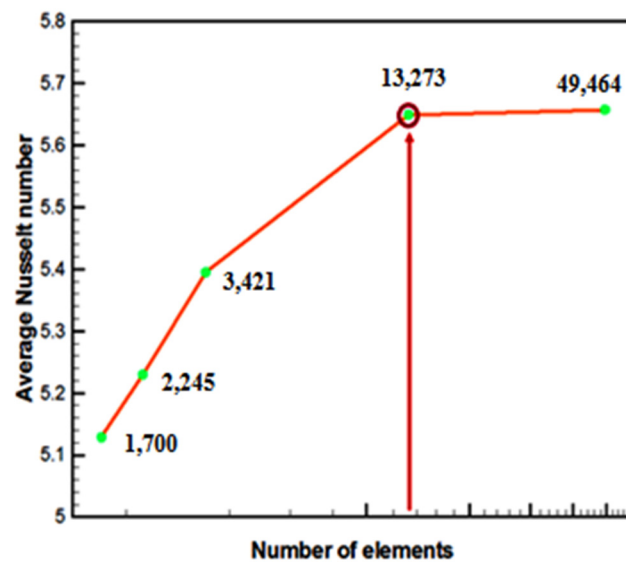


Figure 2. Grid measurement for various elements.

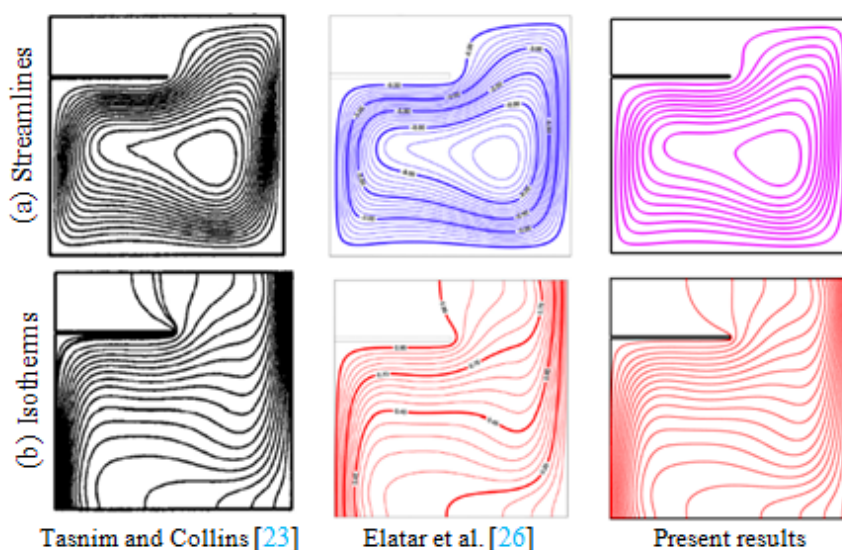
6. Code Validation

To verify an exactness of the existing model's analytical outcomes, the global Nusselt number onward right cool surface was compared among the results manifested by Elatar et al. [26] and Naget al. [22] at $L = 0.20$ and $Ra = 10^6$. The global Nusselt number surveyed in Table 2 shows the excellent agreement of those inquiries within the highest derivation of less than 3.0%.

Table 2. Global Nusselt number on cool wall for $Ra = 10^6$ and $L = 0.20$.

B	0.1	0.02	0.04
Nag et al. [22]	9.033	8.861	8.888
Elatar et al. [26]	8.947	8.672	8.710
Present result	8.985	8.783	8.838

Besides, a matching of isotherms and streamlines was adjusted for the instant results with Tasnim and Collins [23] and Elatar et al. [26] at $Ra = 10^5$, $L = 0.5$, $H = 0.75$, and $B = 0.01$, as exhibited in Figure 3. The appearances of streamline are approximately similar. Isotherms can expose the strong adjustment of instant outcomes with Tasnim and Collins [23] and Elatar et al. [26], as viewed in Figure 3.

**Figure 3.** Comparison with streamlines and isotherms.

7. Discussion on Results

In this report, the impact of fin length on mixed convection heat transfer in presence of a magnetic field in a moving wall enclosure attaching vertical fin was executed. The impact of heat variation in wavy shape cavity was scrutinized, and acquiring the following range were the Richardson number ($0.1 \leq Ri \leq 10$), amplitude number ($A = 0.1$) of oscillations ($\lambda = 2$), fin thickness ($B = 0.04$), fin length ($L = 0.25, 0.35$ and 0.45), and fin position ($H = 0.50$), while $Pr = 0.71$, $Ha = 0\text{--}60$, and $Re = 100$ were considered for the flow inside wavy shape enclosure and then demonstrated graphically. The outcomes are presented concerning streamlines in Figure 4, isotherms in Figure 5, and terms of velocity sketches in Figure 6, Nusselt number in Figure 7, global Nusselt number in Figure 8, mean fluid temperature in Figure 9, and fin effectiveness in Figure 10. Figure 4 illustrates that when $Ri = 0.1$ and for all fin surfaces, buoyancy force's strength inside the wavy frame enclosure was significant, and one vortex appears inside an enclosure generated by the moving wall. Again, when $Ri = 1$ and for all fin surfaces, the flow formation was similar to $Ri = 0.1$, but two vortices arose inside the wavy shape cavity: a primary vortex and a minor vortex. Further again, when the Richardson number grew ($Ri = 5$ and 10) and for all fin surfaces, the buoyancy force's strength was more notable significant, and two vortices seemed to move down the right half and left half of the wave frame cavity. The physical fact behind it was that the Richardson numbers and fin length more significantly influenced the buoyancy force affect to the flow region.

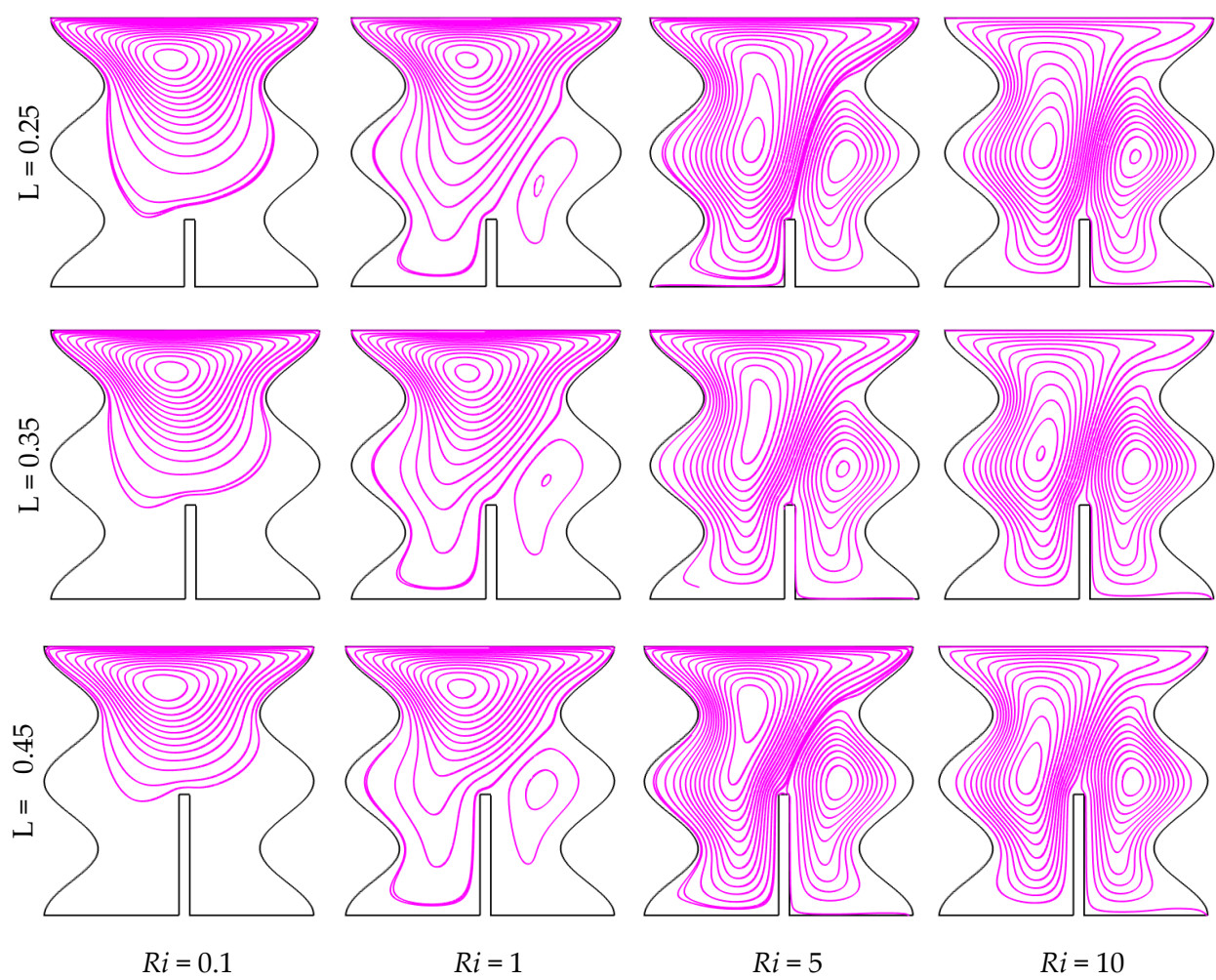


Figure 4. Streamlines for various Ri and L at $Ha = 10$, and $\lambda = 2$.

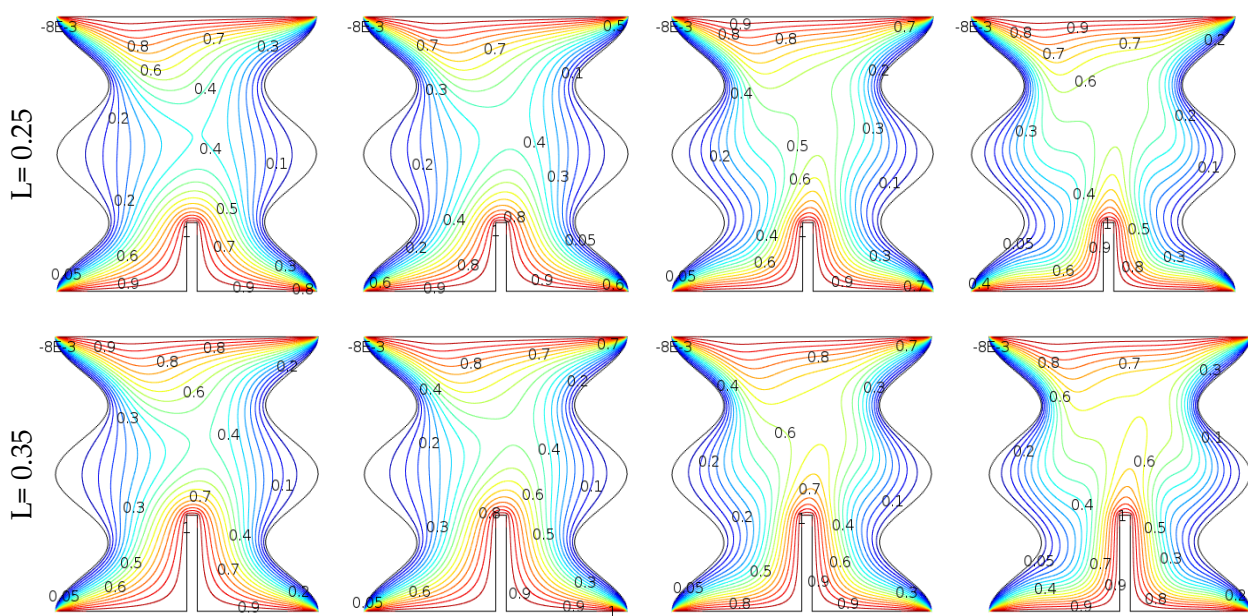
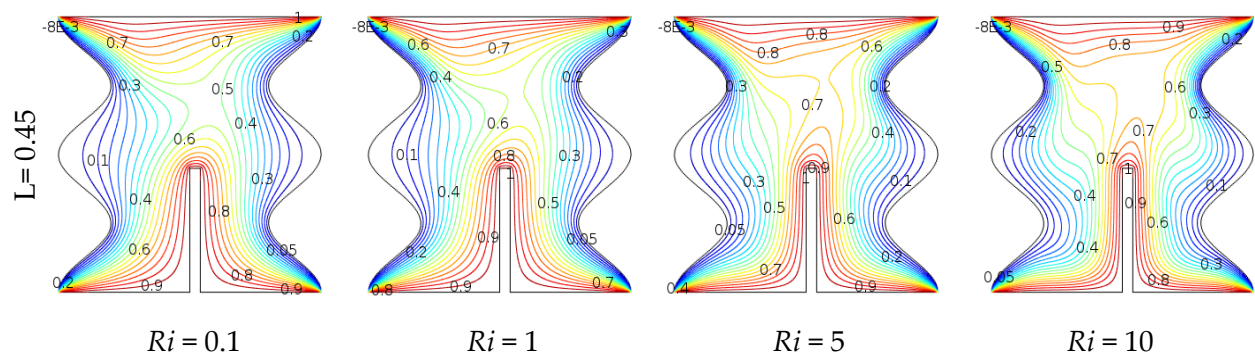
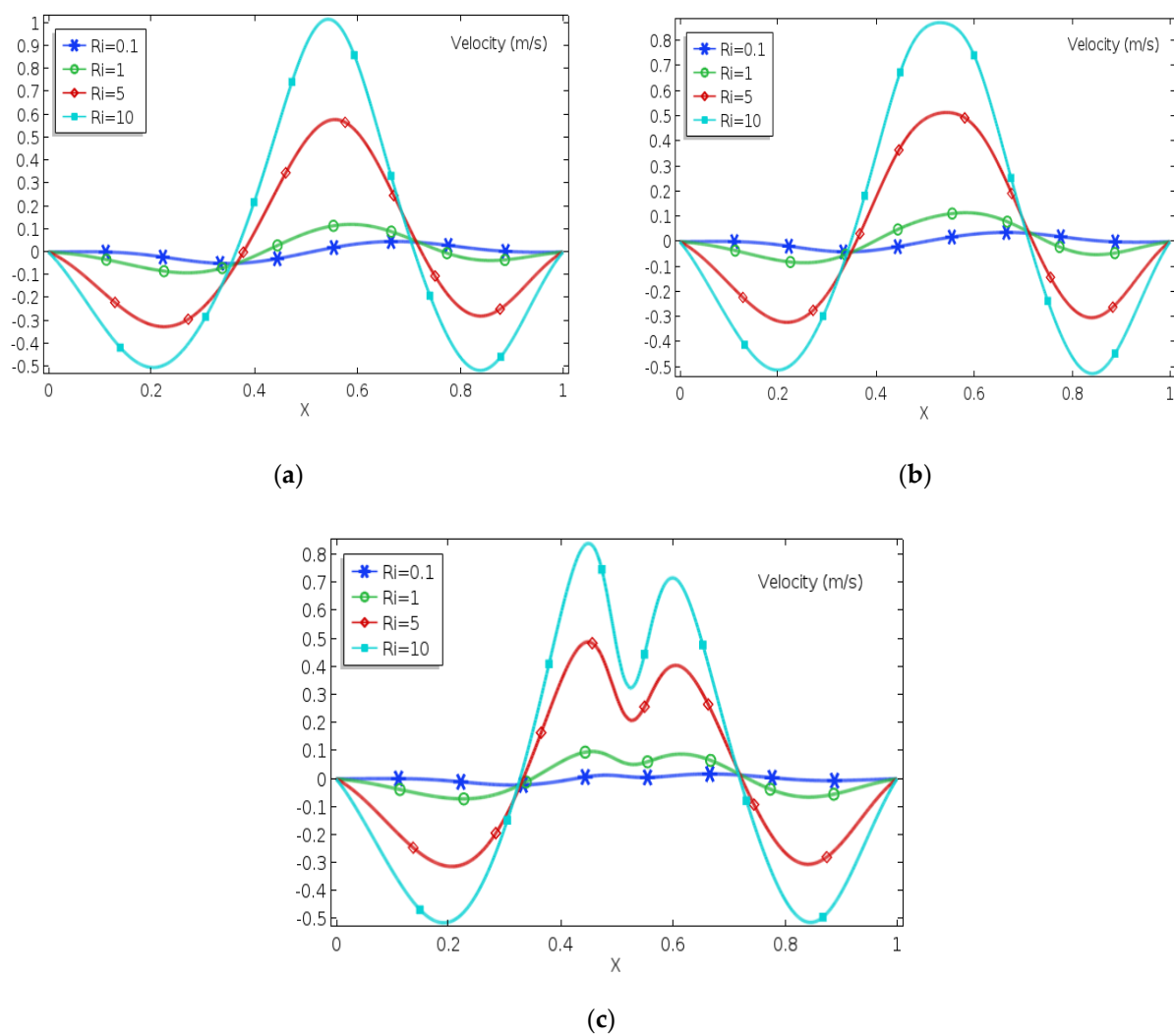


Figure 5. Cont.

**Figure 5.** Isotherms for various Ri and L at $Re = 100$, $Ha = 10$, and $\lambda = 2$.**Figure 6.** Velocity profiles for (a) $L = 0.25$, (b) $L = 0.35$ (c) $L = 0.45$ at $Re = 100$, $Ha = 10$, and $\lambda = 2$.

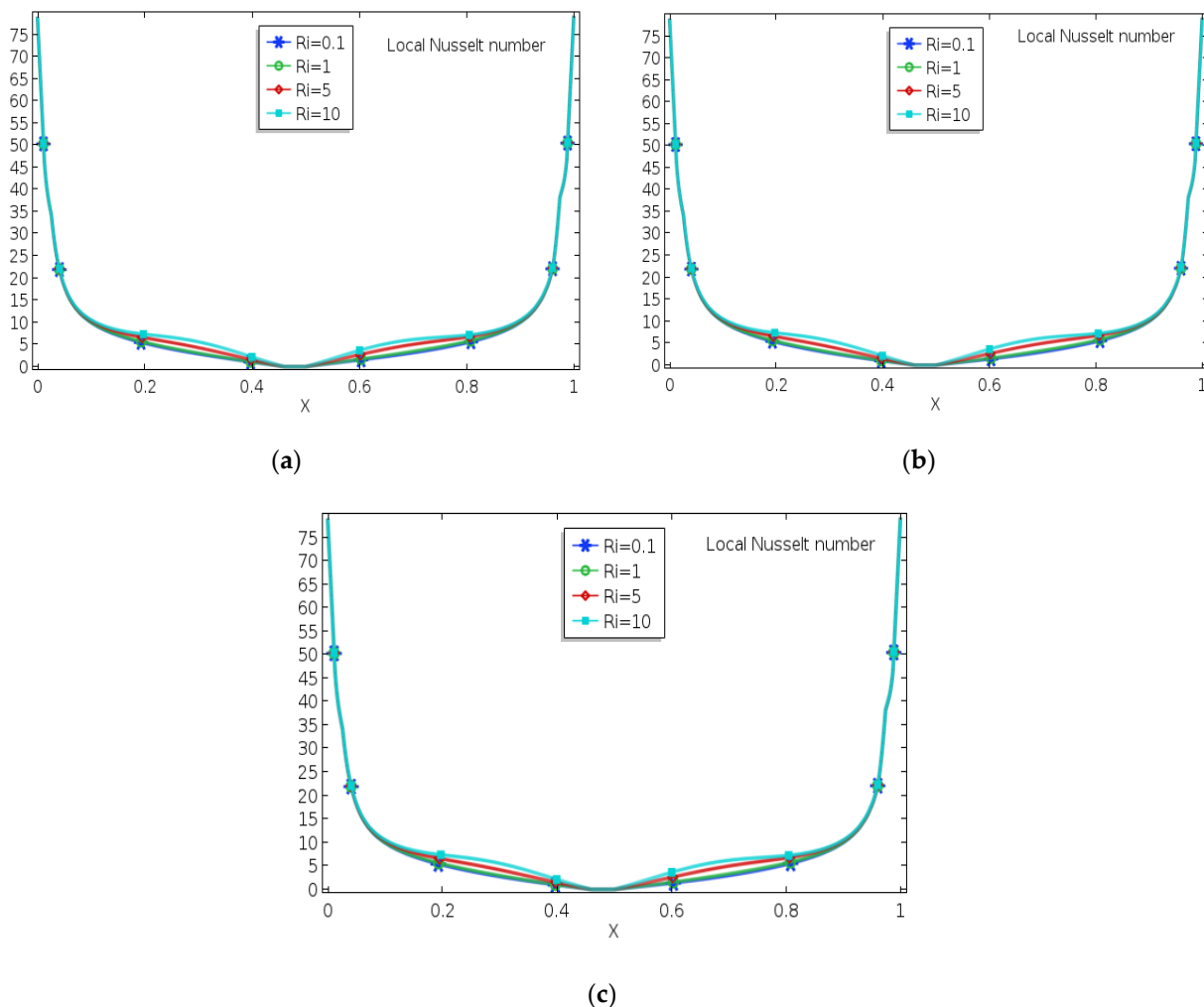


Figure 7. Nu_L for (a) $L = 0.25$, (b) $L = 0.35$ (c) $L = 0.45$ at $Re = 100$ and $\lambda = 2$.

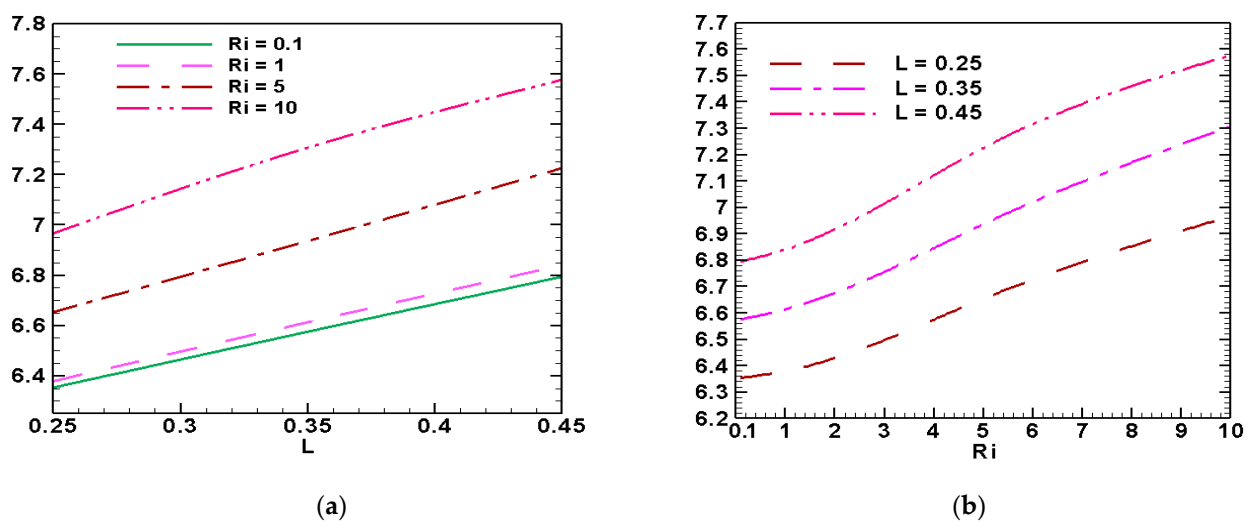


Figure 8. Nu_{av} for (a) several Ri (0.1, 1, 5, and 10) and (b) various L (0.25, 0.35, 0.45) at $Ha = 20$ and $Re = 100$.

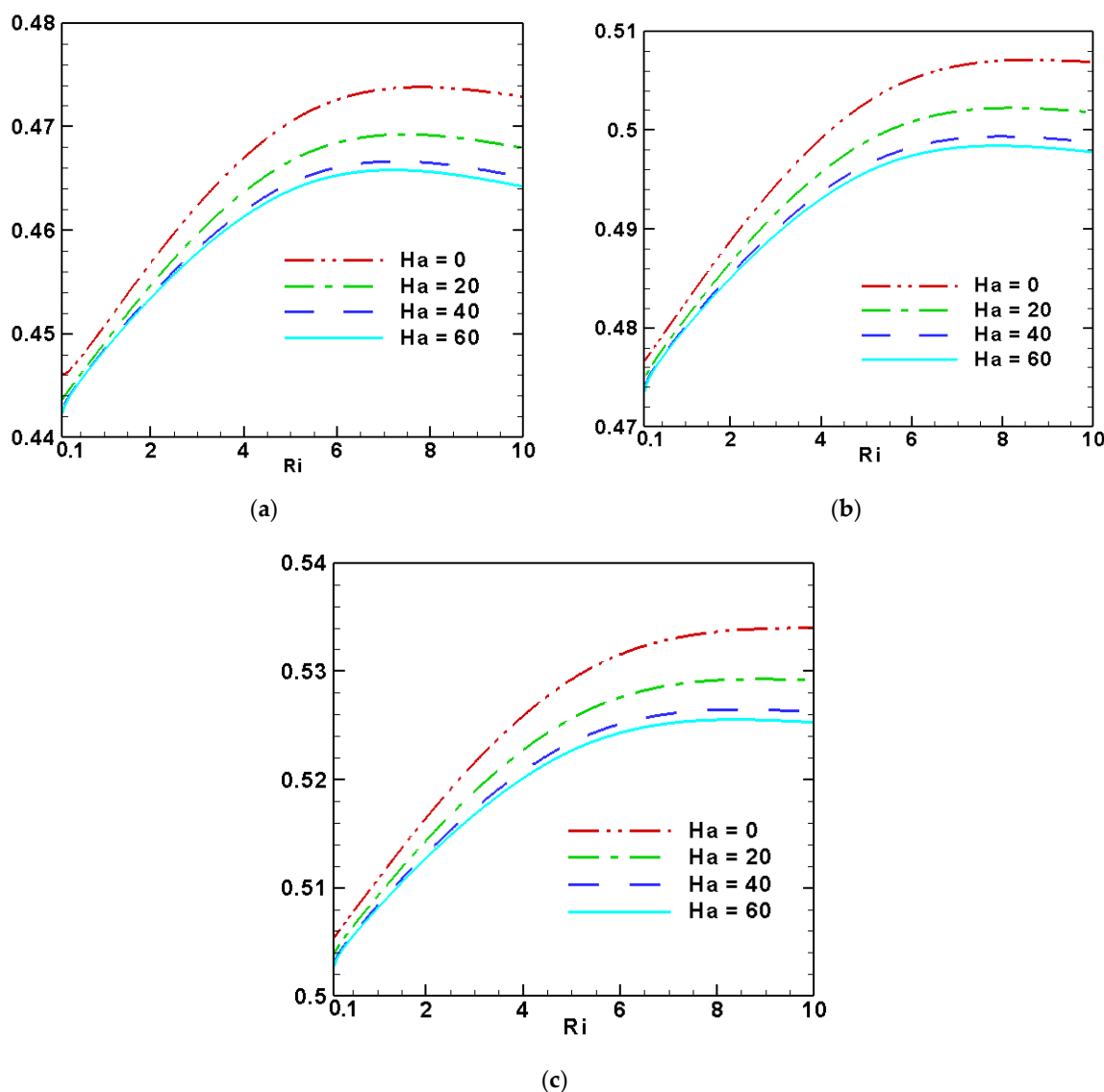


Figure 9. θ_{av} for (a) $L = 0.25$, (b) $L = 0.35$ (c) $L = 0.45$ at $\lambda = 2$ and $Re = 100$.

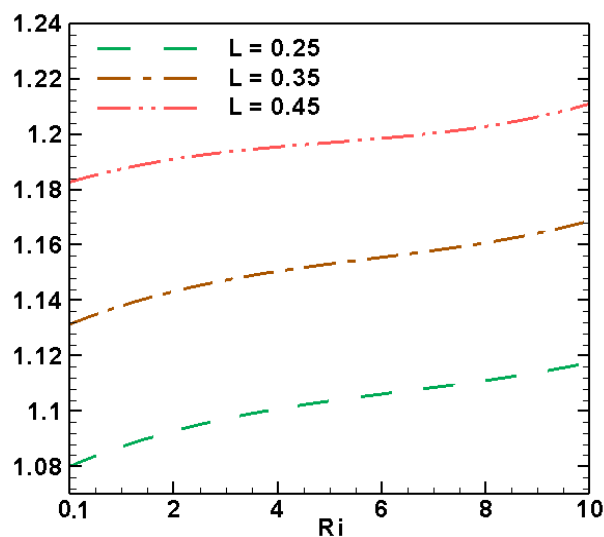


Figure 10. Fin effectiveness for different Ri and L at $Ha = 20$, $Re = 100$, and $\lambda = 2$.

The conduction predominant heat substitution is viewed in isotherms in Figure 5. It is explicit that the thick thermic frame layer exists near the heated walls (top and bottom wall) and a fin surface owing to a lower amount of $Ri = 0.1$, and those become thinner with a higher $Ri = 10$ for all fin surfaces. The curvature shape of isotherms improved with rising Ri and L , and heat lines were compressed to wavy sidewalls and the fin surface, which meant expanding the heat exchange through convection. Impact of velocity outlines onward the horizontal middle line for several fin lengths (L), and Richardson's number (Ri) amidst fin location ($H = 0.50$), $Pr = 0.71$, and $Ha = 10$ of an enclosure is exposed in Figure 6. It can be recognized for lower Ri , velocity outlines have more minor changes. Still, the higher Ri velocity outlines had a more significant change. Further, the positive value of supreme and infimum of the velocity improves with the rising Ri for all baffles. Figure 7 demonstrates Nu_L distribution on the heated wall for distinct fin length (L) and Richardson number (Ri) with fin location ($H = 0.50$), $Pr = 0.71$, $Ha = 10$, and $Re = 100$ of the enclosure. Figure 7 inspects the lower number of a Ri , and Nu_L had an insignificance difference. However, with a higher number of the Ri , Nu_L had a significant difference. In addition, Figure 6 exposed that in the region of the fin tip (position $H = 0.50$), the Nu_L was almost zero. A plot of a global Nusselt number of the right wavy cool surface for the impact of Richardson number (Ri) with separate fin length (L), while the remaining variables value remained fixed, is manifested in Figure 8. From this, Figure 8a demonstrated that the mean Nusselt number rose steadily when fin length extended for a fixed Richardson number. It can be seen from Figure 8b that the global Nusselt number improved steadily when the Richardson number progressed for a singular length of fin. Moreover, extending a Richardson number enhanced a global Nusselt number on the right cool wall. Ri arose at a fixed fin length, buoyancy force develops, and a heat exchange rate was gained.

Figure 9 illustrates a mean fluid temperature (θ_{av}) for several Ri , Ha , and L , while the residual parameter's value was kept constant. Figure 9 marks that mean fluid temperature rose steadily with the progressing Richardson number value when Hartmann number was kept constant. It is also noted that the mean fluid temperature increased when the value of Ha declines. Figure 10 shows fin effectiveness concerning several fin lengths ($L = 0.25$, 0.35 , and 0.45) and Richardson numbers (Ri) at $Pr = 0.71$, $Ha = 20$, and $Re = 100$. Figure 10 inspects the fin effectiveness progress with rising Ri for a distinct fin length. Moreover, for an expanded fin length, convective heat variation began to convert dominant supporting conduction, which produced fin blockage in a significant portion in managing the heat replacement rate. Therefore, a relatively Richardson number was needed to improve the heat discharge rate for each fin length. Table 3 displays the numerical value of the fin effectiveness for different Ri and L at $Ha = 20$ and $Re = 100$. Table 3 mentions that the highest numerical value of heat transfer performance rate of the fin occurred at $L = 0.45$ and $Ri = 10$.

Table 3. Fin effectiveness for various Ri and L at $Ha = 20$ and $Re = 100$.

L	Fin Effectiveness			
	$Ri = 0.1$	$Ri = 1$	$Ri = 5$	$Ri = 10$
0.25	1.081425	1.087349	1.103860	1.118086
0.35	1.132538	1.138264	1.153317	1.169180
0.45	1.183970	1.187686	1.197163	1.211730

8. Conclusions

The impact on flow field and heat transfer characteristics on mixed convection heat transfer under the effect of a magnetic field in a lid driven wavy frame cavity with a vertical fin. The finite element method (FEM) was manipulated to solve relevant governing equations. Comparisons by published literature, including Naget al. [22], Tasnim and Collins [23], and Elatar et al. [26], were accomplished and decided to be an outstanding agreement. The influences of Richardson number, Hartmann number, and various fin lengths inside wavy shape cavity were reported.

- The mixed convection variable Ri had significant impacts on flow field and isotherm contours. Flow field and heat transfer increased with increasing Richardson number for all fin lengths. The best result was seen at $L = 0.45$ for the greatest number of Ri ;
- The impacts of fin length on flow field and temperature characteristics were exposed to be noticeable in all fin lengths. Moreover, the fin length extended the heat transfer rate and the global Nusselt number and mean fluid temperature changes. The best result was found at $L = 0.45$;
- The maximum rate of heat transfer was achieved for the highest Ri with the lowest Ha at the fin length $L = 0.45$;
- Fin effectiveness was improved by raising Ri for distinct fin length. Moreover, the most remarkable fin effectiveness concerning fin length ($L = 0.45$) and Richardson number ($Ri = 10$) was found at Hartmann number ($Ha = 20$).

In view of the present numerical study, the fin surface can significantly enhance the rate of heat transfer performance by increasing convention inside the wavy shape enclosure.

Author Contributions: M.E.-A.-A.: Conceptualization, M.F.-A.-A.; Methodology, M.F.-A.-A.; Software, M.F.-A.-A.; Formal analysis, M.F.-A.-A.; Validation, M.F.-A.-A.; Visualization and Review and editing, M.F.-A.-A., M.Y. and M.M.A.S.; Investigation Resources, M.Y.; Original draft preparation, M.Y.; Data Curation and Original draft preparation, M.N.A. and O.B.; Supervision, M.M.A.S. All authors have read and agreed to the published version of the manuscript.

Funding: This research received no external funding.

Institutional Review Board Statement: Not applicable.

Informed Consent Statement: Not applicable.

Data Availability Statement: Not applicable.

Conflicts of Interest: The authors declare no conflict of interest.

Nomenclatures

A	amplitude
B	dimensionless fin thickness
g	gravitational acceleration
h^*	heat transfer coefficient
h	fin position
H	dimensionless fin position
L	dimensionless fin length
N	dimensionless distance normal to surface coordinates
Nu_{av}	average Nusselt number
Nu_L	local Nusselt number
Ha	Hartmann number
Pr	Prandlt number
Re	Reynold number
Ri	Richardson number
S	dimensionless special coordinate along enclosure surface
ψ, φ	dimensionless velocity in X and Y axis respectively
W	Enclosure height and width

Greek symbols

α	thermal diffusivity
ρ	local density
β	a coefficient of thermal expansion
μ	dynamic viscosity
v	kinematic viscosity
θ	dimensionless temperature
ε	effectiveness
λ	number of oscillations

Subscripts

<i>c</i>	cool
<i>f</i>	fin
<i>h</i>	hot

References

- Azizul, F.M.; Alsabery, A.I.; Hashim, I.; Chamkha, A.J. Impact of heat source on mixed convection flow inside wavy-walled cavity filled with nanofluids via heatline concept. *Appl. Math. Comput.* **2021**, *393*, 125754.
- Das, P.K.; Mahmud, S. Numerical investigation of natural convection inside a wavy enclosure. *Int. J. Therm. Sci.* **2003**, *42*, 397–406. [[CrossRef](#)]
- Misirlioglu, A.; Baytas, A.C.; Pop, I. Natural convection inside an inclined wavy enclosure filled with a porous medium. *Transp. Porous Media* **2006**, *64*, 229–246. [[CrossRef](#)]
- Al-Amiri, A.; Khanafer, K.; Bull, J.; Pop, I. Effect of sinusoidal wavy bottom surface on mixed convection heat transfer in a lid-driven cavity. *Int. J. Heat Mass Transf.* **2007**, *50*, 1771–1780. [[CrossRef](#)]
- Rostami, J. Unsteady natural convection in an enclosure with vertical wavy walls. *Heat Mass Transf.* **2008**, *44*, 1079–1087. [[CrossRef](#)]
- Mansour, M.; El-Aziz, M.A.; Mohamed, R.; Ahmed, S.E. Numerical simulation of natural convection in wavy porous cavities under the influence of thermal radiation using a thermal non-equilibrium model. *Transp. Porous Media* **2011**, *86*, 585–600. [[CrossRef](#)]
- Mushate, K.S. CFD prediction of natural convection in a wavy cavity filled with porous medium. *Glob. J. Res. Eng.* **2011**, *11*, 29–45.
- Nada, E.A.; Chamkha, A.J. Mixed convection flow of a nanofluid in a lid-driven cavity with a wavy wall. *Int. Commun. Heat Mass Transf.* **2014**, *57*, 36–47. [[CrossRef](#)]
- Sheremet, M.A.; Pop, I. Natural convection in a wavy porous cavity with sinusoidal temperature distributions on both side walls filled with a nanofluid: Buongiorno’s mathematical model. *J. Heat Transf.* **2015**, *137*, 072601. [[CrossRef](#)]
- Sheremet, M.; Cimpean, D.; Pop, I. Free convection in a partially heated wavy porous cavity filled with a nanofluid under the effects of Brownian diffusion and thermophoresis. *Appl. Therm. Eng.* **2017**, *113*, 413–418. [[CrossRef](#)]
- Cheong, H.T.; Sivasankaran, S.; Sivasankaran, S.; Bhuvaneswari, M.; Bhuvaneswari, M. Natural convection in a wavy porous cavity with sinusoidal heating and internal heat generation. *Int. J. Numer. Methods Heat Fluid Flow* **2017**, *27*, 287–309. [[CrossRef](#)]
- Asad, M.F.A.; Alam, M.N.; Tunç, C.; Sarker, M.M.A. Heat Transport Exploration of Free Convection Flow inside Enclosure Having Vertical Wavy Walls. *J. Appl. Comput. Mech.* **2021**, *7*, 520–527.
- Fayz-Al-Asad, M.; Alam, M.N.; Ahmad, H.; Sarker, M.M.A.; Alsulami, M.D.; Gepreel, K.A. Impact of a closed space rectangular heat source on natural convective flow through triangular cavity. *Results Phys.* **2021**, *23*, 104011. [[CrossRef](#)]
- Alsabery, A.I.; Tayebi, T.; Chamkha, A.J.; Hashim, I. Effect of rotating solid cylinder on entropy generation and convective heat transfer in a wavy porous cavity heated from below. *Int. Commun. Heat Mass Transf.* **2018**, *95*, 197–209. [[CrossRef](#)]
- Rahman, M.M.; Alim, M.A.; Sarker, M.M.A. Numerical study on the conjugate effect of joule heating and magneto-hydrodynamics mixed convection in an obstructed lid-driven square cavity. *Int. Commun. Heat Mass Transf.* **2010**, *37*, 524–534. [[CrossRef](#)]
- Öztop, H.F.; Sakhrieh, A.; Abu-Nada, E.; Al-Salem, K. Mixed convection of MHD flow in nanofluid filled and partially heated wavy walled lid-driven enclosure. *Int. Commun. Heat Mass Transf.* **2017**, *86*, 42–51. [[CrossRef](#)]
- Ashorynejad, H.R.; Shahriari, A. MHD natural convection of hybrid nanofluid in an open wavy cavity. *Results Phys.* **2018**, *9*, 440–455. [[CrossRef](#)]
- Öztop, H.F.; Salem, K.A.; Pop, I. MHD mixed convection in a lid-driven cavity with corner heater. *Int. J. Heat Mass Transf.* **2011**, *54*, 3494–3504. [[CrossRef](#)]
- Cho, C. Mixed convection heat transfer and entropy generation of Cu-water nanofluid in wavy-wall lid-driven cavity in presence of magnetic field. *Int. J. Mech. Sci.* **2019**, *151*, 703–714. [[CrossRef](#)]
- Mansour, M.A.; Rashad, A.M.; Morsy, Z. MHD free convection and sinusoidal heating in a wavy cavity filled with a heat generation porous medium using Cu-water nanofluids. *Comput. Therm. Sci. Int. J.* **2020**, *12*, 217–232.
- Alsabery, A.I.; Tayebi, T.; Kadhim, H.T.; Ghalambaz, M.; Hashim, I.; Chamkha, A.J. Impact of two-phase hybrid nanofluid approach on mixed convection inside wavy lid-driven cavity having localized solid block. *J. Adv. Res.* **2020**, *30*, 63–74. [[CrossRef](#)]
- Gupta, A.; Garu, A. Analysis heat transfer phenomenon from different fin geometries using CFD simulation in ANSYS. *Int. J. Eng. Sci. Comput.* **2019**, *9*, 23722–23729.
- Nag, A.; Sarkar, A.; Sastri, V.M.K. Natural convection in a differentially heated square cavity with horizontal partition plate on the hot wall. *Comput. Methods Appl. Mech. Eng.* **1993**, *110*, 143–156. [[CrossRef](#)]
- Tasnim, S.H.; Collins, M.R. Numerical analysis of heat transfer in a square cavity with a baffle on the hot wall. *Int. Commun. Heat Mass Transf.* **2004**, *31*, 639–650. [[CrossRef](#)]
- Sun, C.; Yu, B.; Öztop, H.F.; Wang, Y.; Wei, J. Control of mixed convection in lid-driven enclosures using conductive triangular fins. *Int. J. Heat Mass Transf.* **2011**, *54*, 894–909. [[CrossRef](#)]
- Xu, F.; Saha, S.C. Transition to an unsteady flow induced by a fin on the sidewall of a differentially heated air-filled square cavity and heat transfer. *Int. J. Heat Mass Transf.* **2014**, *71*, 236–244. [[CrossRef](#)]

27. Elatar, A.; Teamah, M.A.; Hassab, M.A. Numerical study of laminar natural convection inside square enclosure with single horizontal fin. *Int. J. Therm. Sci.* **2016**, *99*, 41–51. [[CrossRef](#)]
28. Palaniappan, G.; Murugan, M.; Mdalla, Q.M.A.; Doh, B.A.D.H. Numerical investigation of open cavities with parallel insulated baffles. *Int. J. Heat Technol.* **2020**, *38*, 611–621. [[CrossRef](#)]
29. Siddiqui, M.A.; Riaz, A.; Khan, I.; Nisar, K.S. Augmentation of mixed convection heat transfer in a lid-assisted square enclosure utilizing micropolar fluid under magnetic environment: A numerical approach. *Results Phys.* **2020**, *18*, 103245. [[CrossRef](#)]
30. Kouz, W.A.; Muhtady, A.A.; Owhaib, W.; Dahidi, S.A.; Hader, M.; Alghanam, R.A. Entropy generation optimization for rarified nanofluid flows in a square cavity with two fins at the hot wall. *Entropy* **2019**, *21*, 103. [[CrossRef](#)]
31. Shulepova, E.V.; Sheremet, M.A.; Öztop, H.F.; Hamdeh, N.A. Mixed convection of $\text{Al}_2\text{O}_3\text{-H}_2\text{O}$ nanoliquid in a square chamber with complicated fin. *Int. J. Mech. Sci.* **2020**, *165*, 105192. [[CrossRef](#)]
32. Hussain, S.; Jamal, M.; Geridonmez, B.P. Impact of fins and inclined magnetic field in double lid-driven cavity with Cu-water nanofluid. *Int. J. Therm. Sci.* **2021**, *161*, 106707. [[CrossRef](#)]
33. Asad, M.F.A.; Sarker, M.M.A.; Hossain, M.A. Numerical investigation of MHD mixed convection heat transfer having vertical fin in a lid-driven square cavity. *AIP Conf. Proc.* **2019**, *2121*, 030023-6.
34. Asad, M.F.A.; Sarker, M.M.A.; Munshi, M.J.H. Numerical investigation of natural convection flow in a hexagonal enclosure having vertical fin. *J. Sci. Res.* **2019**, *11*, 173–183. [[CrossRef](#)]
35. Asad, M.F.A.; Munshi, M.J.H.; Sarker, M.M.A. Effect of fin length and location on natural convection heat transfer in a wavy cavity. *Int. J. Thermofluid Sci. Tech.* **2020**, *7*, 070303.
36. Yavuz, M.; Sene, N. Approximate Solutions of the Model Describing Fluid Flow Using Generalized p -Laplace Transform Method and Heat Balance Integral Method. *Axioms* **2020**, *9*, 123. [[CrossRef](#)]
37. Althobati, S.; Bazighifan, O.; Yavuz, M. Some Important Criteria for Oscillation of Non-Linear Differential Equations with Middle Term. *Mathematics* **2021**, *9*, 346. [[CrossRef](#)]
38. Agarwal, R.P.; Bazighifan, O.; Ragusa, M.A. Nonlinear Neutral Delay Differential Equations of Fourth-Order: Oscillation of Solutions. *Entropy* **2021**, *23*, 129. [[CrossRef](#)]
39. Taylor, C.; Hood, P. A numerical solution of the Navier–Stokes equations using finite element technique. *Comput. Fluids* **1973**, *1*, 73–89. [[CrossRef](#)]
40. Reddy, J.N. *An Introduction to the Finite Element Method*; McGraw-Hill: New York, NY, USA, 1993.